# Uniaxial strain effects on the superconducting transition in Re-doped Hg-1223 cuprate superconductors

Masaki Mito,[1,*] Kazuma Ogata,[1] Hiroki Goto,[1] Kazuki Tsuruta,[1,†] Kazuma Nakamura,[1] Hiroyuki Deguchi,[1] Tomoya Horide,[1] Kaname Matsumoto,[1] Takayuki Tajiri,[2] Hiroshi Hara,[3] Toshinori Ozaki,[3,4] Hiroyuki Takeya,[3] and Yoshihiko Takano[3]

[1]*Graduate School of Engineering, Kyushu Institute of Technology, Kitakyushu 804-8550, Japan*

[2]*Faculty of Science, Fukuoka University, Fukuoka 814-0180, Japan*

[3]*National Institute for Materials Science, Tsukuba 305-0047, Japan*

[4]*School of Science and Technology, Kwansei Gakuin University, Hyogo 669-1337, Japan*

The effects of uniaxial strain and hydrostatic pressure on $Hg_{0.83}Re_{0.18}Ba_2Ca_{2.4}Cu_{3.6}O_{14}$ [$Hg_{0.83}(Re_{0.18})$-1223] were investigated by ac magnetic measurements under stress corresponding to a pressure of 20 GPa at maximum. According to a previous thermal study based on the Ehrenfest relation, in-plane contraction should increase the superconducting transition temperature $T_c$, whereas out-of-plane contraction should decrease $T_c$. This suggests that the increase in $T_c$ under hydrostatic-pressure contraction must be smaller than that under in-plane contraction. However, the present uniaxial-strain experiments revealed enhancement of $T_c$ under both in-plane and out-of-plane contraction, and the largest enhancement was observed under hydrostatic-pressure contraction. According to a band calculation, all contraction styles induce hole doping from the HgO blocks to the $CuO_2$ blocks, and hydrostatic-pressure contraction yields the largest hole doping among three contractions. This behavior explains well a series of changes in $T_c$ in the stress region of below 8 GPa. More specifically, under hydrostatic-pressure contraction, $T_c$ exhibited an increase, a decrease, and another increase with increasing pressure, and this multistep change is similar to that observed in Bi-2223-type cuprate superconductors, suggesting that it is necessary to distinguish the effect of strain on the middle $CuO_2$ plane in the three-$CuO_2$-plane package from that on the outer planes.

## I. INTRODUCTION

Cuprate superconductors (CSCs) are structurally characterized by the stacking structure of the $CuO_2$ layers. A series of studies on Hg-based, Tl-based, and Bi-based CSCs has revealed that the superconducting transition temperature $T_c$ depends on the number of $CuO_2$ layers $m$ in an accumulation unit of $CuO_2$ layers, and $T_c$ is maximum at $m = 3$ in each CSC system [1–6]. Each copper atom in the $CuO_2$ layers is surrounded by several oxygen atoms, for example, forming a $CuO_5$ square pyramid or a $CuO_6$ octahedron. It is widely recognized that the coordination symmetry around the copper atoms also becomes a key factor in determining $T_c$ [7,8]. Given the above background, hydrostatic-pressure contraction has been a useful experimental approach to changing the distance between $CuO_2$ layers, the distance between a unit of $CuO_2$ layers and a buffer layer, and the coordination symmetry around the copper atoms in the $CuO_2$ layer [7]. The former two factors are correlated with the carrier number in the $CuO_2$ layers. Indeed, we cannot conclude that the application of strain by hydrostatic pressure always yields the most suitable structural manipulation for obtaining the highest $T_c$ of the targeted material. The importance of the uniaxial strain for manipulating $T_c$ has recently been recognized [7], for example, in $YBa_2Cu_3O_7$ (Y-123) [9–13], $YBa_2Cu_4O_8$ (Y-124) [13–17], and $HgBa_2CuO_4$ [18]. Selective structural manipulation by uniaxial strain yields physical information regarding the optimal type of strain for optimizing $T_c$. One uniaxial-strain

approach, a thermal approach using the Ehrenfest relation [12,14,18], is valid for evaluating the contribution of the strain along each principal axis under hydrostatic-pressure contraction. However, in this approach, the crystal contracts or expands along all the principal axes, so we obtain selective information along each principal axis when the lattice change is unrestricted. Another approach is the mechanical uniaxial-strain approach, in which real contraction is permitted only along a force vector to avoid the Poisson effect. Here, the elasticity of the target material determines the limit in genuine mechanical uniaxial-strain experiment, whereas the behavior under low stress yields important information for controlling $T_c$.

The Hg-based CSC with $m = 3$, called Hg-1223, has the highest $T_c$ (~130 K) at ambient pressure among all superconductors [2]. Two groups reported that under hydrostatic-pressure contraction using a diamond anvil cell (DAC), the onset of the electrical resistance appeared above 160 K [19,20]. In a recent hydrostatic-pressure experiment using a cubic anvil cell that allows the application of isotropic stress, the $T_c$ value determined via the zero resistance increased to 153 K [21,22]. On the other hand, the thermal approach based on the Ehrenfest relation has suggested that in-plane contraction enhances $T_c$, whereas out-of-plane contraction suppresses $T_c$ [18]. Here, the result of the thermal study suggests that realization of real in-plane contraction could yield a higher $T_c$ of more than 153 K in the above hydrostatic-pressure experiments. We have already confirmed that Y-124 exhibits an increase in $T_c$ independent of the type of contraction in a mechanical uniaxial-strain experiment [15–17], and we are also interested in the difference between hydrostatic pressure and mechanical uniaxial strain in Hg-1223.

---

[*]mitoh@mns.kyutech.ac.jp

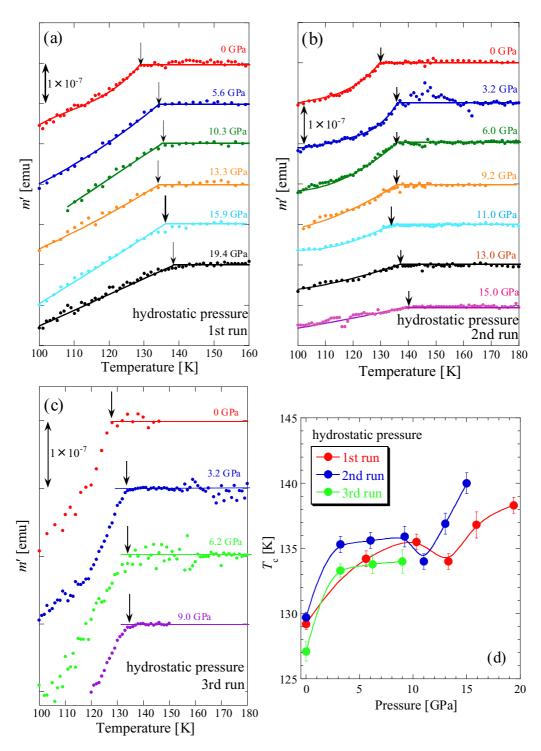[†]Also at JASRI/SPring-8, Hyogo 679-5148, Japan.

FIG. 1. (a–c) Temperature dependence of the in-phase ac magnetic response $m'$ of $Hg_{0.83}(Re_{0.18})$-1223 under hydrostatic-pressure contraction. The number in parentheses indicates the sequence of applied stresses. Arrows represent the $T_c$ values obtained from the point at which $m'$ started to decrease. The pressure-transmitting medium for the first run, shown in (a), was Apiezon J oil, and that for the two runs shown in (b) and (c) was Daphne 7373 oil. (d) Pressure dependence of $T_c$ obtained in the three runs in (a)–(c) against pressurization. The discrete $T_c$ data are connected by a solid guide curve.

In the present study, we investigate the effects of hydrostatic-pressure and mechanical uniaxial-strain contraction of Hg-1223 via Meissner signal measurements and check whether the suggestion from the thermal uniaxial-strain study would be realized under mechanical uniaxial-strain contraction. The electrical resistance is not adequate for the mechanical uniaxial-strain experiment because the electrical contact between the electrodes and the surface of the crystal would become brittle. Indeed, it is technically not easy to detect the Meissner signal of small single crystals under stress at the 10 GPa level, although we have achieved it via the two previous studies on Y-124 [16] and Ca-doped Y-124 [17].

## II. EXPERIMENT

To conduct the mechanical uniaxial-strain experiment on Hg-1223, a single crystal was required. Thus, some of the Hg atoms were replaced with Re atoms, and the preparation of single crystals was promoted by a flux method using $BaZrO_3$ crucibles in a quartz ampoule. The details of crystal growth have been reported elsewhere [23]. It has been shown experimentally that doping with Re suppresses the increase in $T_c$ under hydrostatic pressure [24]. The elemental composition ratio of $Hg_{0.83}Re_{0.18}Ba_2Ca_{2.4}Cu_{3.6}O_{14}$ [$Hg_{0.83}(Re_{0.18})$-1223] was determined by energy-dispersive x-ray spectroscopy. X-ray diffraction (XRD) analysis of the single crystal confirmed that the $c$ axis was aligned perpendicular to the parallelogram plane of the crystal.

The ac magnetic susceptibility was observed using a superconducting quantum interference device magnetometer equipped with an ac option. The frequency and amplitude of the ac field were 10 Hz and 3.9 Oe, respectively. Contraction corresponding to a stress of up to approximately 20 GPa was achieved using a miniature CuBe DAC that consisted of two diamond anvils with flat tips with a diameter of 0.6 mm and a 0.25-mm-thick Re gasket [25]. In the hydrostatic-pressure-type experiment, a liquidlike pressure-transmitting medium, Apiezon J oil or Daphne 7373 oil, was mixed with polycrystalline sample. In the mechanical uniaxial-strain-type experiment, the single crystals were fixed in epoxy resin (Stycast 1266, Ablestick Japan Co., Ltd.) and held in the sample cavity (0.3 mm in diameter), which was made by holing the Re gasket. If the diameter of the sample cavity does not expand, the contraction occurs almost entirely along the load direction. Under these conditions, it is difficult to experimentally determine the magnitude of the strain. Thus, the stress magnitudes in both the hydrostatic-pressure and mechanical uniaxial-strain cases were scaled using a quasipressure $P$ by measuring the fluorescence of ruby [26] located in the sample cavity with the $Hg_{0.83}(Re_{0.18})$-1223 crystals, as in the previous experiments on Y-124 [16] and Ca-doped Y-124 [17]. Thus, we could compare the results of the hydrostatic-pressure -type and mechanical uniaxial-strain-type experiments using the common variable $P$.

Furthermore, to determine the difference between the structural shrinkage under hydrostatic-pressure contraction of non-Re-doped and Re-doped Hg-1223, powder XRD analysis was conducted under hydrostatic pressure of up to $P = 5.3$ GPa at room temperature using a synchrotron radiation XRD system with a cylindrical imaging plate at the Photon Factory at the Institute of Materials Structure Science, High Energy Accelerator Research Organization [27]. The wavelength of the incident x rays was 0.77425 Å. Pressure was applied using a DAC that consisted of two diamond anvils with flat tips with a diameter of 0.8 mm and a 0.3-mm-thick CuBe gasket. The small crystals of $Hg_{0.83}(Re_{0.18})$-1223 passing a sieve with an aperture of 20 $\mu$m were contained in a sample cavity with a diameter of 0.4 mm, along with a ruby used as a manometer and fluorinated oil (FC77, Sumitomo 3M Ltd.) used as the pressure-transmitting medium. The lattice constants were estimated by analyzing a series of diffraction peaks of $Hg_{0.83}(Re_{0.18})$-1223.

## III. FIRST-PRINCIPLES CALCULATION

Density-functional band structure calculations for Hg-1223 were performed using the TOKYO AB-INITIO PROGRAM PACKAGE [28] with plane-wave basis sets, where norm-conserving pseudopotentials [29,30] and the generalized gradient approximation of the exchange-correlation potential [31] were employed. The cutoff energies in the wave function and charge densities were 64 and 256 Ry, respectively, and $15 \times 15 \times 5$ $k$-point sampling was employed. The atomic geometry was fully optimized with fixed lattice parameters. The maximally localized Wannier function [32,33] was used for the Wannier-interpolated band calculations and population analyses. The electronic density of states was calculated by the generalized tetrahedron method [34,35].

## IV. EXPERIMENTAL RESULTS

### A. Hydrostatic pressure

Figures 1(a)–1(c) show the temperature dependence of the in-phase ac magnetic response $m'$ for $Hg_{0.83}(Re_{0.18})$-1223 under hydrostatic-pressure contraction. In the measurements for
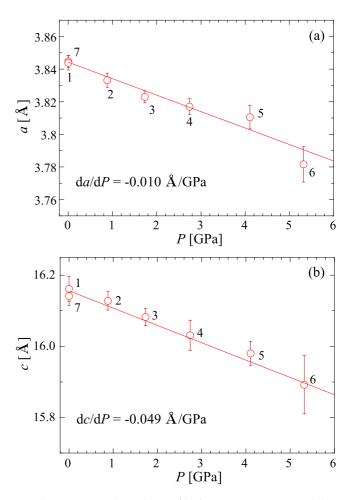


FIG. 2. Pressure dependence of lattice parameters (a) $a$ and (b) $c$ for $Hg_{0.83}(Re_{0.18})$-1223 under hydrostatic-pressure contraction. The straight lines in (a) and (b) have slopes of $da/dP = -1.00 \times 10^{-2}$ Å/GPa (a) and $dc/dP = -4.85 \times 10^{-2}$ Å/GPa (b). The numbers near the plots indicate the order of the measurements.

Fig. 1(a), Apiezon J oil was used as the pressure-transmitting medium, and Daphne 7373 oil was used in those for Figs. 1(b) and 1(c). For instance, in Fig. 1(a), a rapid decrease in $m'$ under ambient pressure was observed at 129 K. The $T_c$ value estimated from the onset of the Meissner signal was enhanced with increasing pressure. For $P = 3$–10 GPa, the increase in $T_c$ was quite small, and $T_c$ reached 135.5 K at 10.3 GPa. Subsequently, $T_c$ decreased slightly, suggesting a parabolic pressure dependence of $T_c$, but it began to increase at around 13 GPa. This phenomenon is also observed in Fig. 1(b), and

a tendency toward temporal saturation in the increase in $T_c$ is also observed in Fig. 1(c). The series of changes in $T_c$ under hydrostatic pressure is summarized in Fig. 1(d). Note that in this material, a qualitative change in $T_c$ does not depend essentially on the type of pressure-transmitting medium.

According to the studies of Yamamoto *et al.* and Takeshita *et al.*, the $T_c$ value of non-Re-doped Hg-1223 is maximum (153 K) at approximately 15 GPa [21,22]. Regarding the $T_c$ value at around 15 GPa, there is a notable difference of approximately 10 K between their data and ours. To elucidate this
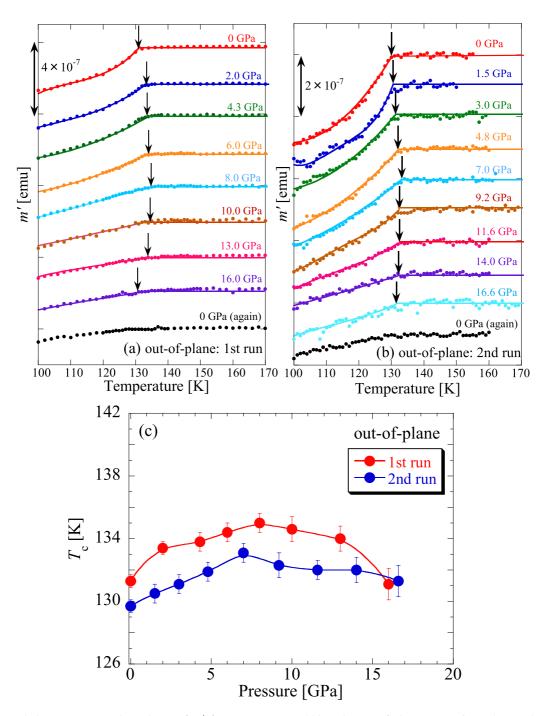


FIG. 3. (a) and (b) Temperature dependence of $m'$ for $Hg_{0.83}(Re_{0.18})$-1223 under out-of-plane contraction. The numbers indicate the sequence of applied stresses. (c) Stress dependence of $T_c$ obtained from the two runs in (a) and (b). A series of $T_c$ data is connected with solid guide curves.

difference, we analyzed the structure of $Hg_{0.83}(Re_{0.18})$-1223 under hydrostatic-pressure contraction. Figure 2 shows the pressure dependence of lattice parameters $a$ and $c$, both of which exhibit linear changes against the pressure of $da/dP = -0.010$ and $dc/dP = -0.049$ Å/GPa. Thus, the shrinkage along the $c$ axis is 5 times that along the $a$ axis. The greater shrinkage along the $c$ axis is qualitatively consistent with the observed behavior of non-Re-doped Hg-1223 [36,37]. For $Hg_{0.83}(Re_{0.18})$-1223, $a$ changes from 3.84(3) to 3.80(0) Å at $P = 5$ GPa, whereas for non-Re-doped Hg-1223, $a$ changes from 3.85(2) to 3.79(3) Å at $P = 5$ GPa [36]. For $Hg_{0.83}(Re_{0.18})$-1223, $c$ changes from 16.1(4)

to 15.9(0) Å at $P = 5$ GPa, whereas for non-Re-doped Hg-1223, $c$ changes from 15.7(6) to 15.2(5) Å at $P = 5$ GPa [36]. The pressure derivative of $a$ for $Hg_{0.83}(Re_{0.18})$-1223, $da/dP = -0.010$ Å/GPa, is quantitatively of the same order as that for non-Re-doped Hg-1223 ($da/dP = -0.012$ Å/GPa [36]). However, the magnitude of the shrinkage along the $c$ axis for $Hg_{0.83}(Re_{0.18})$-1223, $dc/dP = -0.049$ Å/GPa, is about one-third of that for non-Re-doped Hg-1223 ($da/dP = -0.140$ Å/GPa [36]). Furthermore, we stress that the $c$-axis lattice constant for $Hg_{0.83}(Re_{0.18})$-1223 at $P = 5.3$ GPa is at the same level as that for non-Re-doped Hg-1223 at $P = 0$ GPa. Thus, the small compressibility along the $c$ axis
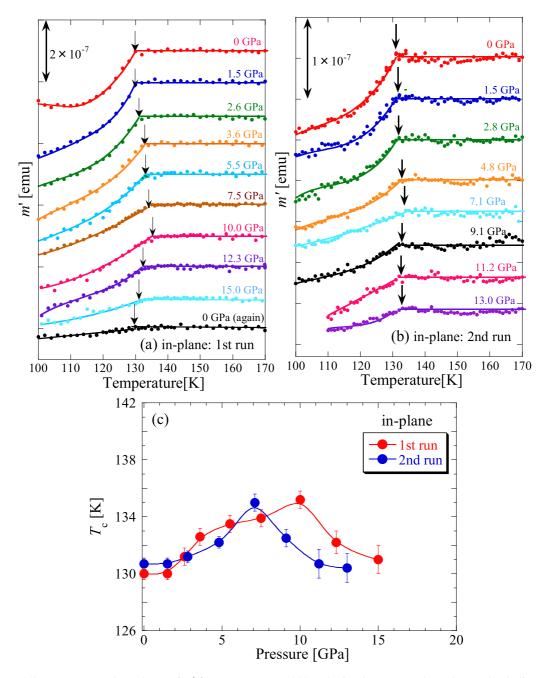


FIG. 4. (a) and (b) Temperature dependence of $m'$ for $Hg_{0.83}(Re_{0.18})$-1223 under in-plane contraction. The number indicates the sequence of applied stresses. (c) Stress dependence of $T_c$ obtained from the two runs in (a) and (b). A series of $T_c$ data is connected with solid guide curves.

for $Hg_{0.83}(Re_{0.18})$-1223 seems to be a promising explanation of the fact that the magnitude of the change in $T_c$ for $Hg_{0.83}(Re_{0.18})$-1223 is smaller than that for non-Re-doped Hg-1223. In the section of discussion, a small change in $T_c$ for $Hg_{0.83}(Re_{0.18})$-1223 will also be discussed from another viewpoint.

### B. Mechanical uniaxial strain

Figures 3(a) and 3(b) show the temperature dependence of $m'$ under out-of-plane contraction, and Fig. 3(c) shows the associated change in $T_c$. In the first run [Fig. 3(a)], the Meissner signal shifts toward higher temperatures, whereas at around $P = 8.0$ GPa, it begins to shift toward low temperatures. The maximum increase in $T_c$ was at most 4 K. Similar behavior was also observed in the second run [Fig. 3(b)], and the increase after the parabolic change seen under hydrostatic-pressure contraction was not observed here.

Figures 4(a) and 4(b) show the temperature dependence of $m'$ under in-plane contraction, and the corresponding change in $T_c$ is shown in Fig. 4(c). In the first run [Fig. 4(a)], the Meissner signal does not move for $P \leqslant 1.5$ GPa; then it shifts toward higher temperatures. The $T_c$ value is maximum at around $P = 10.0$ GPa, above which $T_c$ decreases with increasing $P$. Similar behavior was also observed in the second run [Fig. 4(b)], and its behavior is entirely different from that under out-of-plane contraction, in particular for $P < 2$ GPa. The maximum increase in $T_c$ was approximately 5 K.

Figure 5 shows the stress (pressure) dependence of the change in $T_c$, $\Delta T_c$, of $Hg_{0.83}(Re_{0.18})$-1223 under
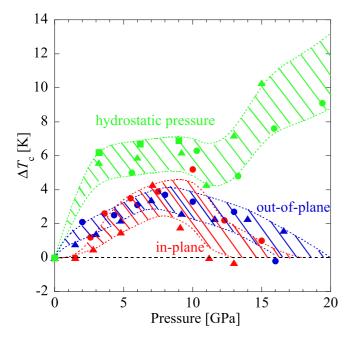


FIG. 5. Stress (pressure) dependence of $\Delta T_c$ for $Hg_{0.83}(Re_{0.18})$-1223 under hydrostatic-pressure, out-of-plane, and in-plane contraction. Even under stress at the 10-GPa level, $\Delta T_c$ is at most 7 K. The distribution of the stress is more than 10% of the mean value to be evaluated. Therefore, we considered a reasonable curve recognizing the scattering in the $T_c$ data. Thus, the tendency under each type of contraction is represented in a certain region by a different color.

hydrostatic-pressure, out-of-plane, and in-plane contraction. The phenomena under the three types of contraction should be distinguished from each other. First, we note that at low pressures (below 2.0 GPa), out-of-plane contraction is important for the increase in $T_c$, whereas in-plane contraction is not an effective positive structural perturbation for higher $T_c$. Hydrostatic-pressure contraction results in a notable increase in $T_c$ in the above pressure region. For $P < 5$ GPa, the change under hydrostatic pressure seems to be explained by a linear combination of those under out-of-plane and in-plane contraction (weighted as 1:2): $\Delta T_c$ (hydrostatic pressure) $\sim 2 \times \Delta T_c$ (in plane) + $\Delta T_c$ (out of plane). It seems that structural elasticity exists for $P < 5$ GPa.

## V. BAND CALCULATION

To remove the uncertainty in the chemical ratio, a first-principles calculation for Hg-1223 instead of $Hg_{0.83}(Re_{0.18})$-1223 was conducted. Also, this system is known to really include excessive oxygen, i.e., $HgBa_2Ca_2Cu_3O_{8+\delta}$, but the occupation of the excessive oxygen $O_\delta$ is small, $\sim 0.2$. Hence, in the present study, we treat the ideal system $HgBa_2Ca_2Cu_3O_8$ with no excessive oxygen for simplicity. Figure 6(a) shows
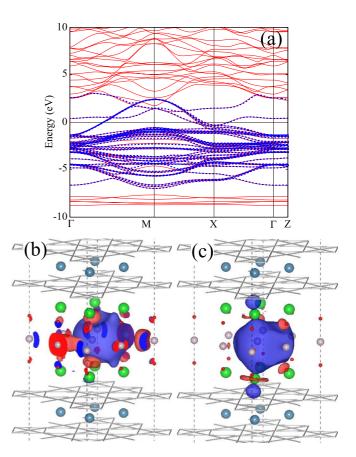


FIG. 6. (a) Density-functional band structure (red curves) for Hg-1223 at $P = 0$. Blue dotted curves describe the Wannier-interpolated bands, where 41 orbitals (24 O $p$, 15 Cu $d$, and 2 Hg $s$ orbitals) are considered. The calculated real-space Hg $s$ Wannier functions are shown in (b) and (c), where they are localized around the positions $(0, 0, 0)$ and $(\frac{1}{2}, \frac{1}{2}, 0)$ in lattice coordinates. Note that the atomic Hg position in the crystal is only $(0, 0, 0)$.
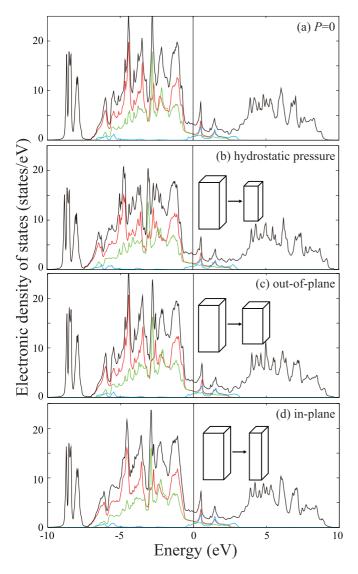
FIG. 7. Calculated electronic density of states for Hg-1223 under (a) ambient pressure and under (b) hydrostatic-pressure, (c) out-of-plane, and (d) in-plane contraction. For (b)–(d), the compression ratio $\alpha$ is 0.98, and a schematic view of the contraction deformation is depicted in the inset of each panel. The electron population obtained by integrating over the considered energy scale is shown in each panel. The total electron population can be obtained by adding the populations in O, Cu, and Hg. Red, green, and blue curves represent the local DOSs based on the O $p$, Cu $d$, and Hg $s$ Wannier orbitals, respectively.

our calculated band structure (red solid curves) of Hg-1223 at $P = 0$. The blue dotted curves are the Wannier-interpolated bands. We found that the original band structures near the Fermi level are represented well by a 41-orbital system consisting of 24 O $p$, 15 Cu $d$, and 2 Hg $s$ orbitals. The initial guesses were prepared as atom-centered Gaussians, but the Gaussian centers for the two Hg orbitals are placed at the $(0, 0, 0)$ and $(\frac{1}{2}, \frac{1}{2}, 0)$ positions in lattice coordinates. Figures 6(b) and 6(c) show the resulting two Hg $s$ Wannier functions.

Figure 7 compares the electronic density of states (DOS) of the different crystal configurations [$P = 0$, hydrostatic
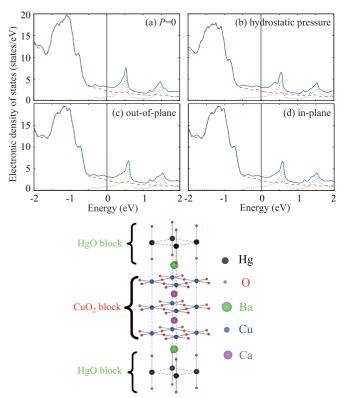


FIG. 8. Magnified view of the density of states for Hg-1223 (a) at ambient pressure and under (b) hydrostatic-pressure, (c) out-of-plane, and (d) in-plane contraction. For (b)–(d), the compression ratio $\alpha$ is 0.98. The total DOS (blue solid curve) is decomposed into two parts, the CuO$_2$ (red dashed curve) and HgO (green dotted one) blocks. The definition of the block is drawn in the bottom panel.

pressure, out of plane, and in plane in Figs. 7(a)–7(d), respectively]. For Figs. 7(b)–7(d), the compression ratio $\alpha$ is 0.98, and a schematic view of the contraction deformation is depicted in the inset of each panel. The local DOSs based on the O $p$, Cu $d$, and Hg $s$ Wannier orbitals are also displayed as red, green, and blue curves, respectively. Each local DOS is the sum over the related orbitals (e.g., the local O DOS is the sum of the 24 O $p$ local DOSs). First, the band structure at $P = 0$ indicates that the orbital of Hg and those of Cu and O contribute to the Fermi surface [38]. Also, the peaks around 0.5 eV are formed by the Hg and O orbitals, which suggests that, for the low-energy band near the Fermi level, the Hg orbital is hybridized with apical oxygen orbitals near the Hg site (see below).

Figure 8 shows a magnified view of the DOS around the Fermi level. In this plot, the total DOS is decomposed into two parts. One is the DOS contributed by the CuO$_2$ block, and the other is that of the HgO block. The definition of each block is drawn in the bottom part of Fig. 8. The block DOS is calculated as the sum of the atomic DOS belonging to each block. Interestingly, the HgO-block DOS (green dotted curves) exhibits an appreciable configuration dependence; the tail of the HgO DOS is extended under contraction, indicating that the electronic population of the HgO block would increase under contraction, or, equivalently, the contraction can be effective for hole doping in the CuO$_2$ block. This trend is observed for

TABLE I. Population analysis based on the maximally localized Wannier orbitals. The population $N$ is calculated for the $CuO_2$ and HgO blocks. For the definition of each block, see the bottom panel of Fig. 8. The results with the different compression conditions are compared; that is, the populations at $P = 0$ (ambient pressure) are compared with those under hydrostatic-pressure, out-of-plane, and in-plane contraction. The $\Delta$ column monitors $N(CuO_2) - N(CuO_2)_{P=0}$, which measures the population change in the $CuO_2$ block with the deformation. Note that the total population is 75.

| | $N(CuO_2)$ | $N(HgO)$ | $\Delta$ |
|---|---|---|---|
| $P = 0$ | 62.589 | 12.411 | |
| Hydrostatic pressure | 62.474 | 12.526 | $-0.115$ |
| Out-of-plane contraction | 62.537 | 12.463 | $-0.052$ |
| In-plane contraction | 62.548 | 12.452 | $-0.041$ |

all the contracted configurations, and the hydrostatic-pressure contraction is very appreciable.

To quantify this hole doping, we perform the population analysis. Table I shows the calculated electronic populations for the $CuO_2$ and HgO blocks. We see that the hydrostatic-pressure contraction increases the HgO-block population by $\sim 0.1$ (i.e., it causes effective hole doping to the $CuO_2$ block). The out-of-plane and in-plane contractions also cause the hole doping, but the amount is moderate; it is half the effects of the hydrostatic-pressure compression. Note here that the definition of the population has arbitrariness; it depends on the kinds of the localized orbitals.

The effects of hydrostatic pressure on Hg-1223 have been understood within a framework in which $T_c$ changes as a function of the carrier density: The increase in $T_c$ is associated with the hole-carrier change from underdoped to optimal, whereas the decrease in $T_c$ occurs as the carrier doping changes from optimal to overdoped. Hg-1223 with $T_c \sim 130$ K is considered to be in the underdoped region close to the optimal state. Given this framework, it is reasonable to understand that both out-of-plane and hydrostatic-pressure contraction increase $T_c$, whereas $T_c$ does not exhibit any change in the low-stress region under in-plane contraction.

## VI. DISCUSSION

According to Fig. 5, the largest increase in $T_c$ was observed under hydrostatic-pressure contraction. The experimental results suggest that, in particular, for $P < 2$ GPa, out-of-plane contraction (i.e., that along the $c$ axis) is more necessary than in-plane contraction (i.e., that along the $ab$ plane). The largest increase in $T_c$, however, requires additional in-plane contraction under the circumstances to enable out-of-plane contraction as well (i.e., hydrostatic-pressure contraction). Indeed, the importance of in-plane contraction was suggested in a theoretical study of a Hg-based CSC with $m = 1$ (Hg-1201) [39] as well as a thermal study of Hg-1223 and Hg-1201 [18]. The in-plane contraction brings about the elongation of the $CuO_5$ pyramid or $CuO_6$ octahedron along the $c$ axis. The theoretical study for Hg-1201 indicates that the above elongation of the $CuO_6$ octahedron increases the energy difference between the $d_{x^2-y^2}$ and $d_{z^2}$ orbitals [39]. The $d$-wave

superconductivity seems to be more stabilized by the decrease in the contribution of the $d_{z^2}$ orbital.

Actually, our first-principles calculations suggest that Hg-1223 has an additional degree of freedom relevant to the $T_c$ modification; that is, the carrier in the $CuO_2$ block can be controlled by the pressure. More specifically, the Hg orbital and the Cu and O orbitals contribute to the Fermi surface. The Hg orbital has a van Hove singularity on the high-energy side near the Fermi level, as does the O site, which is assumed to be apical oxygen existing near Hg. It is reasonable to suppose that via this apical oxygen, carriers (holes) are transferred from the Hg orbitals to the $CuO_2$ planes. In considering the carriers contributing the superconductivity, it is reasonable to divide the stacking structure into the HgO block consisting of Hg and apical oxygen and the $CuO_2$ block consisting of three $CuO_2$ planes. When we consider the charge transfer between the HgO blocks and $CuO_2$ blocks, hydrostatic-pressure contraction exhibits the most prominent hole doping from the HgO blocks into the $CuO_2$ blocks. Consequently, under both out-of-plane and in-plane contraction, hole doping into the $CuO_2$ site occurs, whereas their effects are about half of that by hydrostatic-pressure contraction. This behavior can explain a series of changes in $T_c$ in the stress region below 8 GPa. Thus, the results of both the ac magnetic measurements and first-principles calculations indicate that out-of-plane contraction as well as in-plane contraction is valid to manipulate the carrier density toward optimal density, and hydrostatic-pressure contraction is the most suitable for changing the carrier density. Thus, in Hg-1223, the interesting superconducting properties reflecting the three-layer structure appear. We also note that the hydrostatic-pressure contraction is also the best method to maintain the structural stability of the three-layer stacking structure of the $CuO_2$ planes in Hg-1223.

Next, we discuss the three-step change (an increase, a decrease, and another increase) in $T_c$ for $Hg_{0.83}(Re_{0.18})$-1223 under hydrostatic-pressure contraction. A similar feature was observed in Bi-2223 with $m = 3$ [40]. It was understood by considering two types of change in the carriers; here, we propose the scenario shown in Fig. 9. Generally, it is known in multilayered cuprates that the carrier density of the upper and lower (outer) $CuO_2$ planes, which has fivefold oxygen coordination, is larger than that of the middle (inner) $CuO_2$ plane, which has fourfold oxygen coordination with no apical oxygen [41–44]. The carriers in outer $CuO_2$ planes are transformed from underdoped to optimal to overdoped values, whereas that of the inner $CuO_2$ plane should follow these changes. The outer $CuO_2$ planes are more sensitive to pressure than the inner one since the outer $CuO_2$ planes are closer to the blocking charge reservoir layer. In Hg-1223 without Re, a parabolic change in $T_c$ has been observed [22], and a maximum $T_c$ of 153 K was obtained at around 15 GPa [21,22]. We suppose that the difference in the carrier density between the outer $CuO_2$ planes and the inner $CuO_2$ plane is enhanced by inserting Re into the Hg site near the outer $CuO_2$ planes. After a maximum $T_c$ at around 8 GPa ($\sim P_c$), $T_c$ decreases slightly, but it begins to increase again under further hydrostatic-pressure contraction corresponding to 12–13 GPa. For $P < 12$ GPa, the change in $T_c$ is governed by the outer $CuO_2$ planes, whereas for $P > 13$ GPa, it is controlled by the inner $CuO_2$ plane with a carrier density near the optimal
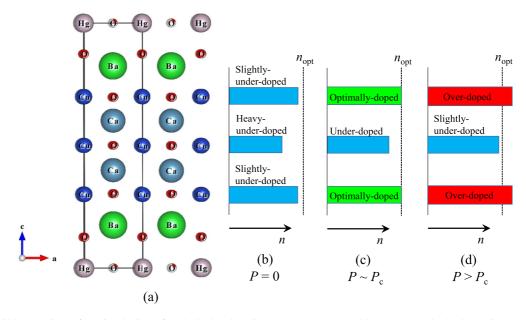
FIG. 9. Possible overview of carrier doping of each CuO$_2$ plane in the Hg$_{0.83}$(Re$_{0.18}$)-1223 system under hydrostatic-pressure contraction. (a) Structure of the unit cell and carrier doping level at (b) $P = 0$, (c) $P \sim P_c$, and (d) $P > P_c$.

level. It is experimentally known that an imbalance between the carrier density at the outer CuO$_2$ planes and that at the inner CuO$_2$ plane brings about the suppression of $T_c$ [43]. Indeed, $T_c$ of Hg$_{0.83}$(Re$_{0.18}$)-1223 is slightly lower than that of Hg-1223, suggesting that the above imbalance in Hg$_{0.83}$(Re$_{0.18}$)-1223 is larger than that in Hg-1223. If the above imbalance in Hg$_{0.83}$(Re$_{0.18}$)-1223 would not become smaller even under pressure, it is reasonably understood that the pressure-induced enhancement of $T_c$ in Hg$_{0.83}$(Re$_{0.18}$)-1223 is smaller than that in Hg-1223.

Finally, the stability of the Meissner signal is discussed. In Y-124 and Y(Ca)-124, remarkable suppression of the Meissner signal has often been observed under a stress at the 10-GPa level [16,17]. The Meissner signal of Hg$_{0.83}$(Re$_{0.18}$)-1223 seems to be notably stable among those of the CSCs, perhaps because the CuO$_2$ package consists of three CuO$_2$ planes.

The present results showed that it is important to maintain the structural package of three CuO$_2$ planes and also to contract the package along the $c$ axis. Indeed, ceramic CSCs are weak against strain, and in terms of selective manipulation, out-of-plane contraction is more useful and effective in $m = 1$ systems such as Hg-1201 than in $m = 3$ systems such as Hg-1223. In Hg-1223, the stability of the structural package of three CuO$_2$ planes must be considered. The superconductivity of multiple CuO$_2$ planes should be sensitive to the strain, and the effect of the strain should appear in the change in the Meissner signal. In single-layered CSCs such as Hg-1201, multiorbital analysis of the effects of uniaxial and hydrostatic pressure on $T_c$ was performed by Sakakibara *et al.* [39]. There has been one thermal study that can be compared with the experimental results. A similar study of Hg-1201 is desirable as the next experiment.

## VII. CONCLUSION

We investigated the change in the $T_c$ value of Re-doped Hg-1223 [Hg$_{0.83}$(Re$_{0.18}$)-1223] under uniaxial and hydrostatic-pressure contraction. Two mechanical uniaxial-strain experiments showed that, in the stress region of less than approximately 2 GPa, out-of-plane contraction (along the $c$ axis) is more effective as the initial contraction for increasing $T_c$ than in-plane contraction (along the $ab$ plane). In the present high-pressure experiments, hydrostatic-pressure contraction is the most effective approach to increasing $T_c$, suggesting that a further effective increase in $T_c$ requires that the structural homogeneity of the three-CuO$_2$-plane package be maintained. Because an elastic limit exists in Hg-1223, it is not easy to maintain the structural homogeneity at pressures at the 10-GPa level, and we can understand the above usefulness of hydrostatic-pressure contraction as a real phenomenon. A band calculation suggests that under all contractions, hole doping into the CuO$_2$ blocks occurs, whereas hydrostatic-pressure contraction exhibits the largest hole doping into the CuO$_2$ blocks. These behaviors are consistent with the change in $T_c$ for $P < 8$ GPa. Under hydrostatic-pressure contraction, $T_c$ exhibited a two-step increase, and we surely have to distinguish the effects of the strain on the outer CuO$_2$ planes from those on the inner one. This effect originates from doping of Re into the Hg site near the outer CuO$_2$ planes of the three-CuO$_2$-plane package. To compare the results of hydrostatic-pressure and mechanical uniaxial-strain contraction with those for thermal uniaxial-strain contraction in a more ideal system, Hg-1201, which has a one-CuO$_2$-plane package, might be more suitable than Hg-1223.

[1] S. N. Putilin, E. V. Antipov, O. Chmaissem, and M. Marezio, Nature (London) **362**, 226 (1993).

[2] A. Shilling, M. Cantoni, J. D. Guo, and H. R. Ott, Nature (London) **363**, 56 (1993).

[3] A. Iyo, Y. Tanaka, H. Kito, K. Yasuharu, H. Matsuhata, K. Tokiwa, and T. Watanabe, Physica C (Amsterdam, Neth.) **460–462**, 436 (2007).

[4] S. Ideta, K. Takashima, M. Hashimoto, T. Yoshida, A. Fujimori, H. Anzai, T. Fujita, Y. Nakashima, A. Ino, M. Arita *et al.*, Phys. Rev. Lett. **104**, 227001 (2010).

[5] X. Chen and C. Gong, Phys. Rev. B **59**, 4513 (1999).

[6] X. Chen, Z. Xu, J. Wang, Z. Jiao, and Q. Zhang, Chem. Phys. Lett. **258**, 1 (1996).

[7] J. S. Schilling, in *Handbook of High-Temperature Superconductivity*, edited by J. R. Schrieffer (Springer, New York, 2007), pp. 427–462.

[8] Y. Ohta, T. Tohyama, and S. Maekawa, Phys. Rev. B **43**, 2968 (1991).

[9] M. F. Crommie, A. Y. Liu, A. Zettl, M. L. Cohen, P. Parilla, M. F. Hundley, W. N. Creager, S. Hoen, and M. S. Sherwin, Phys. Rev. B **39**, 4231 (1989).

[10] U. Welp, M. Grimsditch, S. Fleshler, W. Nessler, J. Downey, G. W. Crabtree, and J. Guimpel, Phys. Rev. Lett. **69**, 2130 (1992).

[11] G. L. Belenky, S. M. Green, A. Roytburd, C. J. Lobb, S. J. Hagen, R. L. Greene, M. G. Forrester, and J. Talvacchio, Phys. Rev. B **44**, 10117 (1991).

[12] C. Meingast, O. Kraut, T. Wolf, H. Wühl, A. Erb, and G. Müller-Vogt, Phys. Rev. Lett. **67**, 1634 (1991).

[13] M. Mito, H. Matsui, T. Imakyurei, H. Deguchi, T. Horide, K. Matsumoto, A. Ichinose, and Y. Yoshida, Appl. Phys. Lett. **104**, 102601 (2014); **104**, 199902 (2014).

[14] C. Meingast, J. Karpinski, E. Jilek, and E. Kaldis, Physica C (Amsterdam, Neth.) **209**, 591 (1993).

[15] M. Mito, T. Imakyurei, H. Deguchi, K. Matsumoto, T. Tajiri, H. Hara, T. Ozaki, H. Takeya, and Y. Takano, J. Phys. Soc. Jpn. **81**, 113709 (2012).

[16] M. Mito, T. Imakyurei, H. Deguchi, K. Matsumoto, H. Hara, T. Ozaki, H. Takeya, and Y. Takano, J. Phys. Soc. Jpn. **83**, 023705 (2014).

[17] M. Mito, H. Matsui, H. Goto, H. Deguchi, K. Matsumoto, H. Hara, T. Ozaki, H. Takeya, and Y. Takano, J. Phys. Soc. Jpn. **85**, 024711 (2016).

[18] F. Hardy, N. J. Hillier, C. Meingast, D. Colson, Y. Li, N. Barišić, G. Yu, X. Zhao, M. Greven, and J. S. Schilling, Phys. Rev. Lett. **105**, 167002 (2010).

[19] L. Gao, Y. Y. Xue, F. Chen, Q. Xiong, R. L. Meng, D. Ramirez, C. W. Chu, J. H. Eggert, and H. K. Mao, Phys. Rev. B **50**, 4260 (1994).

[20] M. Monteverde, C. Acha, M. Núñez-Regueiro, D. A. Pavlov, K. A. Lokshin, S. N. Putilin, and E. V. Antipov, Europhys. Lett. **72**, 458 (2005).

[21] N. Takeshita, A. Yamamoto, A. Iyo, and H. Eisaki, J. Phys. Soc. Jpn. **82**, 023711 (2013).

[22] A. Yamamoto, N. Takeshita, C. Terakura, and Y. Tokura, Nat. Commun. **6**, 8990 (2015).

[23] S. Ueda, J. Shimoyama, S. Horii, and K. Kishio, Physica C (Amsterdam, Neth.) **452**, 35 (2007).

[24] M. T. D. Orlando, A. G. Cunha, E. V. L. de Mello, H. Belich, E. Baggio-Saitovitch, A. Sin, X. Obradors, T. Burghardt, and A. Eichler, Phys. Rev. B **61**, 15454 (2000).

[25] M. Mito, M. Hitaka, T. Kawae, K. Takeda, T. Kitai, and N. Toyoshima, Jpn. J. Appl. Phys. **40**, 6641 (2001).

[26] G. J. Piermarini, S. Block, J. D. Barnett, and R. A. Forman, J. Appl. Phys. **46**, 2774 (1975).

[27] A. Fujiwara, K. Ishii, T. Watanuki, H. Suematsu, H. Nakao, K. Ohwada, Y. Fujii, Y. Murakami, T. Mori, H. Kawada *et al.*, J. Appl. Cryst. **33**, 1241 (2000).

[28] J. Yamauchi, M. Tsukada, S. Watanabe, and O. Sugino, Phys. Rev. B **54**, 5586 (1996).

[29] N. Troullier and J. L. Martins, Phys. Rev. B **43**, 1993 (1991).

[30] L. Kleinman and D. M. Bylander, Phys. Rev. Lett. **48**, 1425 (1982).

[31] J. P. Perdew, K. Burke, and M. Ernzerhof, Phys. Rev. Lett. **77**, 3865 (1996).

[32] N. Marzari and D. Vanderbilt, Phys. Rev. B **56**, 12847 (1997).

[33] I. Souza, N. Marzari, and D. Vanderbilt, Phys. Rev. B **65**, 035109 (2001).

[34] T. Fujiwara, S. Yamamoto, and Y. Ishii, J. Phys. Soc. Jpn. **72**, 777 (2003).

[35] Y. Nohara, S. Yamamoto, and T. Fujiwara, Phys. Rev. B **79**, 195110 (2009).

[36] A. R. Armstrong, W. I. F. David, I. Gameson, P. P. Edwards, J. J. Capponi, P. Bordet, and M. Marezio, Phys. Rev. B **52**, 15551 (1995).

[37] R. Gatt, J. S. Olsen, L. Gerward, I. Bryntse, A. Kareiva, I. Panas, and L. G. Johansson, Phys. Rev. B **57**, 13922 (1998).

[38] D. J. Singh, Phys. Rev. B **48**, 3571 (1993).

[39] H. Sakakibara, K. Suzuki, H. Usui, K. Kuroki, R. Arita, D. J. Scalapino, and H. Aoki, Phys. Rev. B **86**, 134520 (2012).

[40] X. Chen, V. V. Struzhkin, Y. Yu, A. F. Goncharov, C. Lin, H. Mao, and R. J. Hemley, Nature (London) **466**, 950 (2010).

[41] H. Kotegawa, Y. Tokunaga, K. Ishida, G.-q. Zheng, Y. Kitaoka, H. Kito, A. Iyo, K. Tokiwa, T. Watanabe, and H. Ihara, Phys. Rev. B **64**, 064515 (2001).

[42] H. Mukuda, S. Shimizu, A. Iyo, and Y. Kitaoka, J. Phys. Soc. Jpn. **81**, 011008 (2012).

[43] S. Iwai, H. Mukuda, S. Shimizu, Y. Kitaoka, S. Ishida, A. Iyo, H. Eisaki, and S.-i. Uchida, JPS Conf. Proc. **1**, 012105 (2014).

[44] H. Mukuda, S. Shimizu, A. Iyo, and Y. Kitaoka, J. Phys. Soc. Jpn. **85**, 083701 (2016).